Current-Driven Skyrmion Dynamics and Drive-Dependent Skyrmion Hall Effect in an Ultrathin Film

Roméo Juge[1,*] Soong-Geun Je[1], Dayane de Souza Chaves,[2] Liliana D. Buda-Prejbeanu,[1]
José Peña-Garcia,[2] Jayshankar Nath,[1] Ioan Mihai Miron,[1] Kumari Gaurav Rana,[1] Lucia Aballe,[3]
Michael Foerster,[3] Francesca Genuzio,[4] Tevfik Onur Menteş[4] Andrea Locatelli,[4]
Francesco Maccherozzi,[5] Sarnjeet S. Dhesi,[5] Mohamed Belmeguenai,[6] Yves Roussigné,[6]
Stéphane Auffret,[1] Stefania Pizzini,[2] Gilles Gaudin,[1] Jan Vogel,[2] and Olivier Boulle[1,†]

[1]*Univ. Grenoble Alpes, CNRS, CEA, Grenoble INP,[‡] IRIG-Spintec, 38000 Grenoble, France*
[2]*Univ. Grenobles Alpes, CNRS, Institut Néel, 38000 Grenoble, France*
[3]*ALBA Synchrotron Light Facility, 08290 Cerdanyola del Vallès, Barcelona, Spain*
[4]*Elettra-Sincrotrone Trieste S.C.p.A., 34149 Basovizza, Trieste, Italy*
[5]*Diamond Light Source Ltd., Didcot OX11 0DE, United Kingdom*
[6]*Laboratoire des Sciences des Procédés et des Matériaux, CNRS, Université Paris 13, 93430 Villetaneuse, France*

Magnetic skyrmions are chiral spin textures that hold great promise as nanoscale information carriers. Since their first observation at room temperature, progress has been made in their current-induced manipulation, with fast motion reported in stray-field-coupled multilayers. However, the complex spin textures with hybrid chiralities and large power dissipation in these multilayers limit their practical implementation and the fundamental understanding of their dynamics. Here, we report on the current-driven motion of Néel skyrmions with diameters in the 100-nm range in an ultrathin Pt/Co/MgO trilayer. We find that these skyrmions can be driven at a speed of $100 \, \text{m s}^{-1}$ and exhibit a drive-dependent skyrmion Hall effect, which is accounted for by the effect of pinning. Our experiments are well substantiated by an analytical model of the skyrmion dynamics as well as by micromagnetic simulations including material inhomogeneities. This good agreement is enabled by the simple skyrmion spin structure in our system and a thorough characterization of its static and dynamical properties.

DOI: 10.1103/PhysRevApplied.12.044007

I. INTRODUCTION

Magnetic skyrmions are fascinating spin textures that have recently attracted considerable attention. Their peculiar topology and nanometer size confer on them quasi-particlelike properties that, combined with their ability to be moved by an electrical current, make them promising candidates for the storage and manipulation of information. They are envisaged to be information carriers in racetrack memories [1] and logic devices [2] combining high density, thermal stability, and high data flow. Among the different classes of materials hosting skyrmions, sputtered multilayered stacks comprising ultrathin heavy-metal (HM)/ferromagnet (FM) layers combine several interesting features. Their structural-inversion asymmetry along with the large spin-orbit coupling of the HM lead to a large interfacial Dzyaloshinskii-Moriya interaction (DMI),

a key ingredient in the skyrmion stabilization that ensures their homochirality and their Néel nature [3]. In addition, the current-induced spin-orbit torques (SOTs) in these systems are expected to provide an efficient way to drive the skyrmions [4]. In recent years, a concerted effort has led to the observation of stable magnetic skyrmions under ambient conditions in these structures [5–13] as well as their current-driven dynamics [5,8,12,14]. Their topological properties affect their dynamics in a nontrivial manner. Notably, due to their quantized topological charge, magnetic skyrmions are subject to the so-called skyrmion Hall effect (SkHE) [15,16], which leads to their deviation from the trajectory imposed by the current. This dynamical signature of their topology needs to be characterized and taken into account for future applications. Numerous studies of skyrmion dynamics have been focused on multilayers with a large number of repetitions [8,14,16]. In particular, fast motion ($100 \, \text{m s}^{-1}$) of small skyrmions (100 nm) has been reported in [Pt/CoFeB/MgO]$_{15}$ [8,16]. However, in these stray-field-coupled multilayers, the large dipolar fields can outweigh the DMI and stabilize twisted

*romeo.juge@protonmail.com
†olivier.boulle@cea.fr
‡Institute of Engineering Univ. Grenoble Alpes

spin structures with a nonuniform chirality across the film thickness [17–19]. This leads to a complex current-driven dynamics due to layer-dependent SOTs and topologies [20,21]. Notably, these hybrid textures may not conserve their topological charge during motion at high current density and therefore may not be skyrmions which cannot be described by existing models [20]. Furthermore, for a given current density, a larger Joule dissipation is also expected, since it scales with the total film thickness. Therefore, the demonstration of fast current-driven skyrmion motion in nanometer-thick film systems is a prerequisite for the development of low-power skyrmion-based devices and for a simple understanding of their dynamics.

In this work, we report on the observation of the current-driven motion of isolated magnetic skyrmions in an ultrathin Pt/Co/MgO film. Previously, we have shown that this system exhibits a large interfacial DMI and hosts homochiral Néel skyrmions at room temperature [7]. Here, we find that these skyrmions, with diameters in the 100-nm range, move at a velocity up to 100 m s^{-1} and that the SkHE is markedly drive dependent. These observations are complemented by a detailed characterization of the static and dynamical properties of the stack. These measurements and the simple skyrmion spin structure in our system allow us to approach a quantitative comparison with the prediction of the Thiele equation at high current density. Real-scale micromagnetic simulations including material inhomogeneities reproduce the observed drive dependence of the skyrmion mobility and the SkHE, allowing the identification of different dynamic regimes. The simulations reveal that the drive dependence of the SkHE is not accounted for by the fieldlike SOT (FL-SOT), as previously claimed [16], but by pinning, which greatly impacts the skyrmion dynamics at low current density.

II. RESULTS AND DISCUSSION

A. Experimental results

We study the current-driven dynamics of magnetic skyrmions in a sputter-deposited Ta(3)/Pt(3)/Co(0.9)/MgO (0.9)/Ta(2) film (thicknesses in nanometers) at room temperature, using the high-spatial-resolution photoemission electron microscopy combined with x-ray magnetic circular dichroism (XMCD-PEEM). The sample is patterned into 3-μm-wide tracks with injection pads consisting of Ti(10 nm)/Au(100 nm), as represented in Fig. 1(a). An external out-of-plane magnetic field $\mu_0 H_z \approx -5$ mT is applied on the initially demagnetized configuration in order to stabilize skyrmions with a core magnetized along $+\hat{\mathbf{z}}$. In Figs. 1(b)–1(e) and 1(f)–1(j), two sequences of images display the characteristic current-driven motion of the skyrmions. Between each acquisition, a single 11-ns current pulse of amplitude $J = 5.6 \times 10^{11} \text{ A m}^{-2}$ is
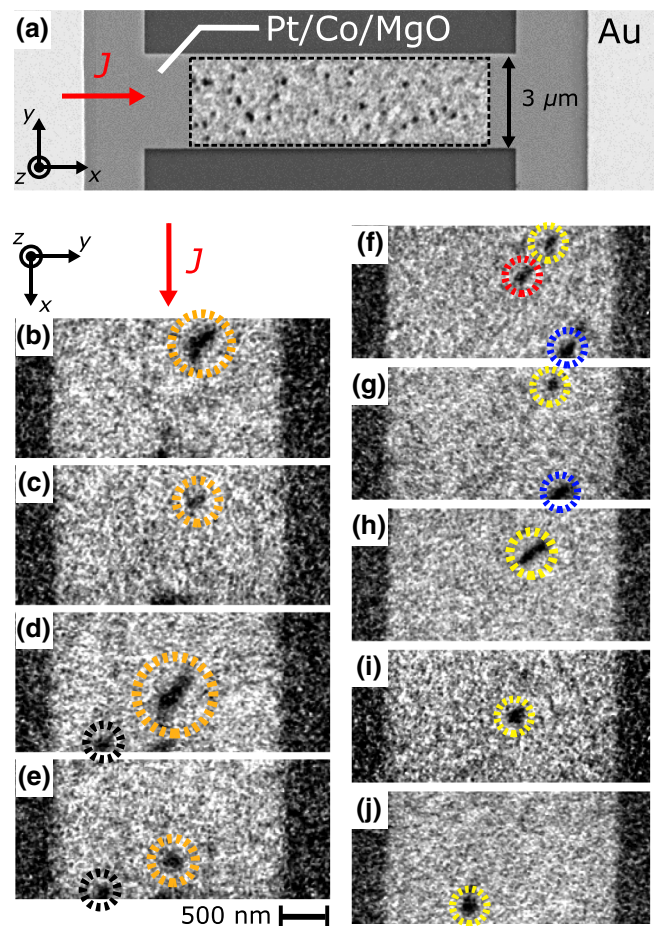

FIG. 1.   (a) A scanning electron microscopy (SEM) image of the device, consisting of a 3-μm-wide Pt/Co/MgO track contacted with Ti/Au pads for the current injection. A XCMD-PEEM image (black dashed rectangle) showing isolated skyrmions in the track is superimposed on the SEM image. (b)–(e),(f)–(j) Two distinct sequences of images. Each image is acquired after a single 11-ns current pulse. In both cases, the charge current is flowing along $+\hat{\mathbf{x}}$ with $J = 5.6 \times 10^{11} \text{ A m}^{-2}$. The applied magnetic field is $\mu_0 H_z \approx -5$ mT.

injected along $+\hat{\mathbf{x}}$. Overall, some skyrmions exhibit a net motion of several hundreds of nanometers along the current direction, that is, against the electron flow (yellow and orange circles). The same directionality is also observed for skyrmions with the opposite core polarity, when $H_z > 0$. In addition, these skyrmions experience a net motion perpendicular to the current direction, which is the signature of the SkHE. This kind of motion is consistent with the current-driven dynamics of left-handed Néel skyrmions governed by the spin Hall effect (SHE), as discussed hereafter. However, it also exhibits a stochastic character, with events of nucleation (black circle) and annihilation (red and blue circles). In addition, the sequences (b)–(e) and (f)–(j) reveal that the skyrmion displacements are not identical for each current pulse. Finally, some skyrmions

appear to be distorted after a current pulse and sometimes acquire an elongated shape. This stochastic behavior can be attributed to the presence of pinning sites obstructing the skyrmion motion [22,23]. This local disorder can also explain the large dispersion observed in the skyrmion size and shape [24–26], with a measured average effective diameter $d_{Sk} = 156 \pm 45$ nm (see Sec. 1.4 within the Supplementary Material [27]).

Despite this irregular motion, systematic measurements of the current-induced displacements averaged over a large number of skyrmions allow us to extract an average skyrmion velocity and skyrmion Hall angle (SkHA)—namely, the angle Θ_{SkH} between the current and the skyrmion motion directions [see Figs. 2(a)–2(c)]. Figure 2(d) displays the dependence of the skyrmion velocity on the current density. The velocity is calculated as the total displacement divided by the measured pulse width (8 ns and 11 ns in our experiments) and then averaged over multiple events at the same current density. The thermal drift between each acquisition is corrected from larger images using the right-angled corner of the track [see Fig. 1(a)]. Note that below a certain current density, highlighted by the shaded area in Fig. 2(d), no significant displacement is observed after a single current pulse. Above $J = 3.5 \times 10^{11}$ A m^{-2}, the skyrmion velocity increases monotonically with the current density and reaches 100 m s^{-1} for $J = 6.8 \times 10^{11}$ A m^{-2}. This value is comparable to the largest velocities recorded for skyrmions of similar size in stray-field-coupled multilayers [8]. However, the use of a single repetition allows to lower the power dissipation by one order of magnitude. Furthermore, as previously mentioned, the current injection also leads to a motion perpendicular to the current direction. The direction of deflection with respect to the current direction is unchanged when reversing the current direction [see Figs. 2(a)–2(c)], which is characteristic of the SkHE. The measurements [Fig. 2(e), black squares] reveal that the SkHA depends on the skyrmion velocity and exhibits a monotonic increase up to approximately 50°.

In the following, we discuss and interpret these results in the light of the Thiele model as well as micromagnetic simulations. For this purpose, we realize a detailed characterization of the static and transport properties of the Pt/Co/MgO stack to approach a quantitative comparison with the experimental results. Details of the different measurements are given in the Supplementary Material [27] and the parameters extracted are summarized in Table I.

B. Comparison with the analytical model

The experimental results are first compared with the prediction of the Thiele equation [28], which captures the dynamics of magnetic skyrmions well. Under the assumption that the skyrmions behave as rigid spin textures, the steady-state velocity **v** results from an equilibrium between
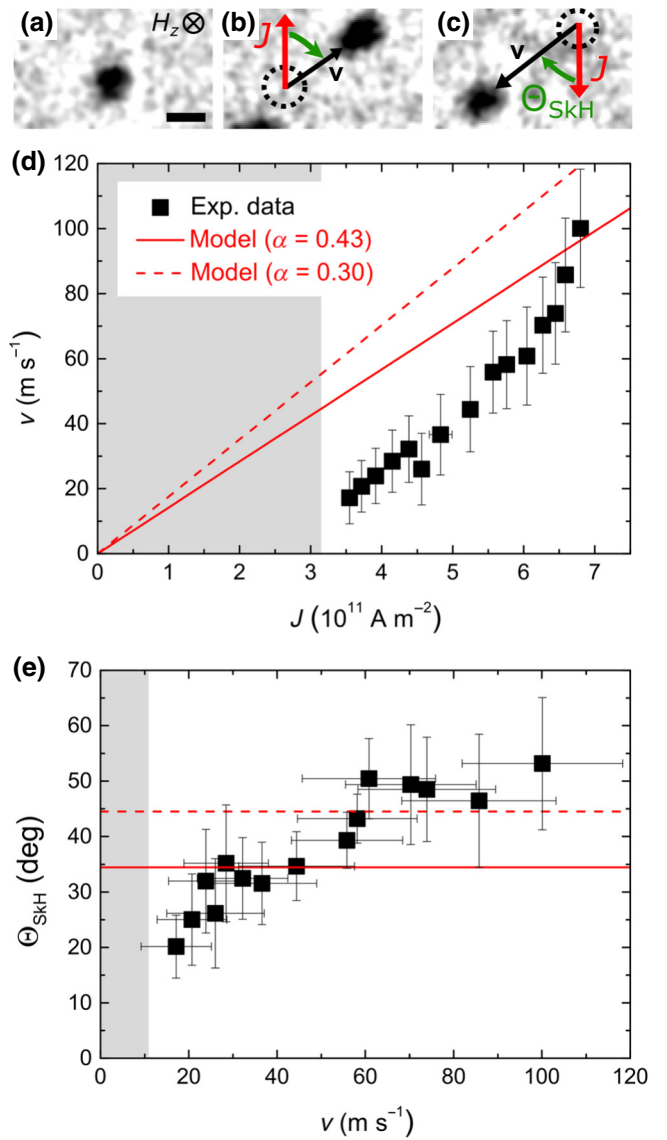

FIG. 2. (a)–(c) A sequence of XMCD-PEEM images showing a skyrmion after two consecutive 8-ns current pulses with opposite polarities (the scale bar is 200 nm). The skyrmion Hall angle (SkHA) Θ_{SkH} is defined as the angle between the current and the skyrmion-motion directions. (d) The skyrmion velocity as a function of the current density. (e) The SkHA as a function of the skyrmion velocity. The red solid lines and red dashed lines are the analytical skyrmion velocity and the SkHA calculated from Eqs. (2) and (3) using the parameters given in Table I for $\alpha = 0.43$ and $\alpha = 0.30$, respectively. The error bars denote the sum of the systematic measurement error and the standard deviation. The shaded areas highlight the regime for which no significant displacement is observed after a single current pulse.

different forces acting on the skyrmion:

$$\mathbf{F}_{DL} + \mathbf{G} \times \mathbf{v} - \alpha\mathbf{D} \cdot \mathbf{v} = \mathbf{0}. \quad (1)$$

Here, $\mathbf{F}_{DL}$ is the force due to the current injection. In the case of HM/FM ultrathin films, the force results from

TABLE I. A summary of the parameters used in the analytical model and the simulations. The saturation magnetization M_s and the uniaxial anisotropy K_u obtained from SQUID magnetometry measurements. The DMI parameter D measured using Brillouin-light-scattering (BLS) spectroscopy. The damping parameter α extracted from the DW mobility in the field-driven steady-flow regime. The exchange constant A extracted from micromagnetic simulations and BLS measurements. The DW width parameter Δ deduced from micromagnetic simulations. The average skyrmion radius R measured at $\mu_0 H_z \approx -5$ mT. The DL-SOT and FL-SOT effective fields per unit current density, C_{DL} and C_{FL} respectively (given in mT per 10^{11} A m^{-2}), extracted from harmonic Hall voltage measurements. The current density is calculated from the measured current transmitted through the device, assuming that it flows uniformly in Pt(3)/Co(0.9), owing to the larger resistivity of the Ta(3) underlayer. Additional details can be found in the Supplementary Material [27].

M_s (MA m^{-1})	K_u (MJ m^{-3})	$\|D\|$ (mJ m^{-2})	α	A (pJ m^{-1})	Δ (nm)	R (nm)	$C_{DL} 10^{-14}$ (T A^{-1} m^2)	$C_{FL} 10^{-14}$ (T A^{-1} m^2)
1.42 ± 0.05	1.34 ± 0.12	1.27 ± 0.04	0.43 ± 0.08	16 ± 6	11.5	78 ± 23	2.1	0.9

the action of the so-called dampinglike spin-orbit torque (DL-SOT): the charge current flowing in the Pt layer is converted into a spin current due to the SHE. The spin accumulation at the Pt/Co interface leads to a torque acting on the Co magnetization. In the case of Pt/Co/MgO, since the spin Hall angle (SHA) is positive for Pt [29] and skyrmions are of Néel type and exhibit a left-handed chirality [7], the symmetries of the DL-SOT impose that the resulting force drives the skyrmion in the current direction (i.e., opposite to the electron flow) [12]. In addition, the topology of the skyrmion leads to a gyrotropic force, $\mathbf{G} \times \mathbf{v}$, where $\mathbf{G} = G\hat{\mathbf{z}}$ is the gyrovector, the sign of which depends only on the topological charge N_{Sk}, with $G \propto N_{Sk}$ [28,30]. For instance, in Figs. 2(a)–2(c), $\mathbf{G}$ points in the $-\hat{\mathbf{z}}$ direction. This second term thus describes the SkHE. The third term describes the dissipative force, in which $\mathcal{D}$ is the dissipative tensor and α is the Gilbert damping parameter. Note that the effect of the FL-SOT is neglected. Indeed, the action of the FL-SOT is equivalent to that of an external magnetic field applied in a direction perpendicular to the current direction and a spatially homogeneous magnetic field does not result in a force on a rigid skyrmion in Thiele's approach. This approximation is justified in the next section by micromagnetic simulations. Although simple, this equation captures most of the physical ingredients that drive the skyrmion dynamics and is particularly relevant in our ultrathin films with a homogeneous homochiral Néel spin configuration across the film thickness. Assuming that the skyrmion has a radial 360° Bloch wall profile [31], a rotational symmetry, and that its radius R is much larger than the domain wall (DW) width parameter Δ ($R \gg \Delta$), the skyrmion velocity and the SkHA can be written as follows [12,32]:

$$v = \frac{\gamma \pi}{4} \frac{R}{\sqrt{\left(\frac{\alpha R}{2\Delta}\right)^2 + 1}} C_{DL} J, \quad (2)$$

$$\tan \Theta_{SkH} = \frac{2\Delta}{\alpha R}. \quad (3)$$

Here, γ is the gyromagnetic ratio, α is the Gilbert damping parameter, J is the current density flowing in the Pt layer, and C_{DL} is the effective field (per unit current density) associated with the DL-SOT. We use the parameters listed in Table I. The analytical solution for the velocity is plotted in Fig. 2(d) (red solid line): it reveals a relatively good agreement with the experimental data at high current density, considering that the velocity depends critically on all the aforementioned parameters. Nevertheless, we observe that the experimental values are smaller than the one predicted by the Thiele equation at low current density. A similar observation has been pointed out in the study of the current-driven dynamics of DWs in Pt/Co/AlO$_x$ ultrathin films [33]. It can be accounted for by the effect of pinning on the skyrmion dynamics, not taken into account in this simple model, which is expected to lead to a thermally activated regime at low drive current, characterized by smaller velocities. This indicates that the skyrmion dynamics in our experiments is in a depinning regime and this points at the existence of a flow regime for the largest current densities injected.

With regard to the SkHA, we find a value $\Theta_{SkH} = 34°$ $\pm 8°$ using Eq. (3). The uncertainty includes the uncertainty on the skyrmion radius. Note that this value is independent of the skyrmion velocity or the applied current, in sharp contrast with our observations as well as previous experimental studies [15,16]. This disagreement with the experiments can also be explained by the presence of pinning sites [22,23,34–36]. The calculated SkHA (i.e., the steady-flow SkHA) is found to be smaller than the maximum measured values [see Fig. 2(e), red solid line]. However, as detailed in the next section, one expects the SkHA to tend toward the calculated value for large skyrmion velocities. Note that the damping is a key parameter in the calculation of the skyrmion velocity and the SkHA. Here, we use the value $\alpha = 0.43$. It is extracted from field-driven DW dynamics measurements in a Pt/Co(0.63 nm)/MgO film (see Sec. 1.5 within the Supplemental Material [27]). This value is in good agreement with previous DW dynamics experiments in ultrathin Pt/Co/Pt [37] and Pt/Co/AlO$_x$ [33,38] films. To explain

such large damping values, besides the contributions of surface roughness [39] and spin pumping into the Pt layer [40], the presence of Rashba spin-orbit coupling is also predicted to enhance the damping [41]. This additional contribution can be expected in our stack considering the non-negligible FL-SOT (see Table I) and can lead to a significant reduction of the DW and skyrmion velocity as well as the SkHA [42]. We note that the damping parameter is measured in a stack with a slightly thinner Co layer, which is required to stabilize larger domains and drive DWs with an external field. In a thicker Co layer, the different interfacial contributions to the damping mentioned above are expected to decrease. The simplest approximation to account for the change in the Co thickness is to assume that $\alpha \sim 1/t$, leading to $\alpha = 0.30$ for the Pt/Co(0.9 nm)/MgO film used to study the skyrmion dynamics. Accounting for this correction leads to an enhancement of the calculated skyrmion velocity and of the SkHA $\Theta_{\mathrm{SkH}} = 45° \pm 8°$ [see Figs. 2(d) and 2(e), red dashed lines] that provides a better agreement with the experimental results, as it will be justified in the next section.

C. Micromagnetic simulations

To go beyond the assumptions and limitations of the analytical model, we perform micromagnetic simulations using the parameters listed in Table I. Both the DL-SOT and the FL-SOT are taken into account. These torques are given, respectively, by $\mathbf{T}_{\mathrm{DL}} = -\gamma_0 C_{\mathrm{DL}} J \mathbf{m} \times [(\hat{\mathbf{z}} \times \hat{\mathbf{j}}) \times \mathbf{m}]$ and $\mathbf{T}_{\mathrm{FL}} = -\gamma_0 C_{\mathrm{FL}} J \mathbf{m} \times (\hat{\mathbf{z}} \times \hat{\mathbf{j}})$, in which $\gamma_0 = \mu_0 \gamma$, $\mathbf{m}$ is the reduced magnetization vector, $\hat{\mathbf{j}}$ is the unit vector in the current direction, and C_{DL} (C_{FL}) is the measured effective field per unit current density associated with the DL-SOT (FL-SOT) [43]. The simulations are carried out using the MICRO3D code [44]. The geometry consists of a $1040 \times 560 \times 0.9$ nm^3 track with a cell size of $3.2 \times 3.2 \times 0.45$ nm^3. An out-of-plane external field $\mu_0 H_z = -5.4$ mT is applied, which sets the skyrmion radius to 78.8 nm—that is, the experimental value—and thermal fluctuations are neglected. Figures 3(a) and 3(b) show snapshots of the skyrmion dynamics during the application of a current with $J = 2.9 \times 10^{11}$ A m^{-2} and 6.7×10^{11} A m^{-2}, respectively. As indicated by the red arrow, the current is tilted by 45° with respect to the track direction so that the skyrmions move along the track. The simulations reveal that the skyrmion experiences an expansion accompanied by a deformation that becomes more pronounced with increasing driving current. This effect is purely dynamical: when the current is turned off, the skyrmion shrinks back to its original size and recovers its rotational symmetry. In addition, we find that this deformation is independent of the FL-SOT and is therefore only due to the DL-SOT (see Sec. 2.2 within the Supplemental Material [27]). To highlight this effect, we calculate the effective skyrmion
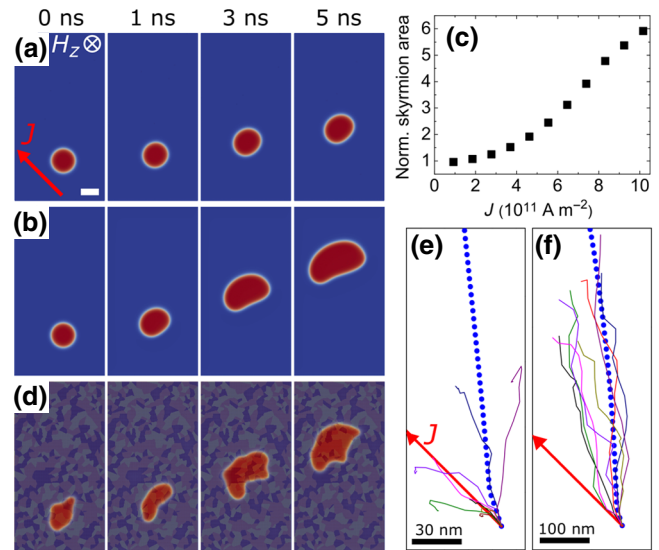

FIG. 3. (a),(b) Sequences of snapshots showing the current-driven dynamics of a skyrmion in an ideal disorder-free film with (a) $J = 2.9 \times 10^{11}$ A m^{-2} and (b) $J = 6.7 \times 10^{11}$ A m^{-2} (the scale bar is 100 nm). (c) The evolution of the skyrmion size as a function of the applied current density (at 5 ns). The size is defined as the area for which $m_z > 0$ (in red), normalized by the area at rest. (d) A sequence of snapshots in a disordered film. The dark grains are region of higher anisotropy and the bright grains those of lower anisotropy. (e),(f) A summary of the trajectories recorded for different grain distributions for (e) $J = 2.9 \times 10^{11}$ A m^{-2} and (f) 6.7×10^{11} A m^{-2}. The blue dotted lines indicate the skyrmion trajectories in the disorder-free scenario. The position of deformed skyrmions is defined as that of their barycenter. The simulations are performed for the experimental parameters listed in Table I with the applied field $\mu_0 H_z = -5.4$ mT.

size, defined as the total area for which $m_z > 0$, normalized by the skyrmion area at rest. Figure 3(c) displays its evolution with the current density. It shows that the skyrmion size increases significantly, in contradiction with the rigid-core assumption of the Thiele model. We note that the simulated skyrmion size matches that of the observed skyrmions and it is significantly larger than the size considered in most studies [4,16,22,23], which could explain why this dynamical effect has not been emphasized before.

To quantify the dynamics of a noncircular skyrmion, we define its position as that of its barycenter. The obtained skyrmion velocity and SkHA are plotted as blue dots in Figs. 4(a) and 4(b) respectively. Remarkably, the simulations are in very good agreement with the simple prediction of the analytical model (red line). This highlights the relevance of discussing our experimental results in the light of the Thiele model. In addition, it emphasizes that the effect of the FL-SOT, which is not taken into account in the model, is not significant in our system. Surprisingly, the DL-SOT-induced expansion and/or deformation does not significantly alter the skyrmion dynamics in the range
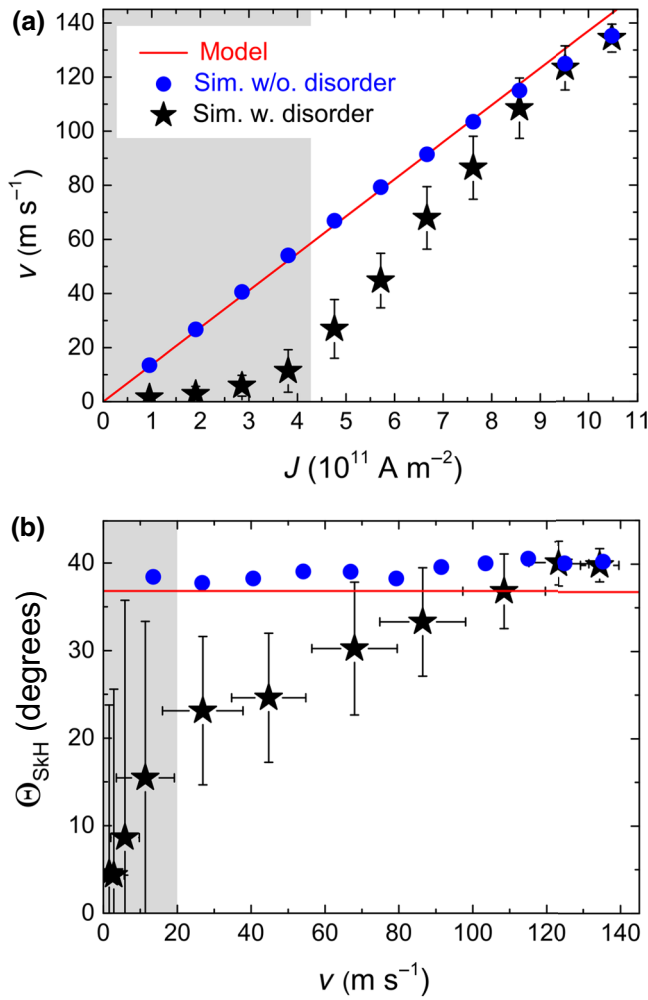
FIG. 4. (a) The skyrmion velocity as a function of the current density in the case of a disorder-free film (blue circles) and in the case of a disordered film (black stars). (b) The SkHA Θ_{SkH} as a function of the skyrmion velocity. The analytical solutions (red solid lines) are calculated from (a) Eq. (2) and (b) Eq. (3) using the parameters given in Table I. To mimic the experimental conditions, the velocity and the SkHA are calculated from the total skyrmion displacement within an 8-ns time window. The error bars denote the standard deviation. The shaded areas highlight the pinned regime.

of current density considered, in spite of the large increase in the skyrmion size [Fig. 3(c)]. Therefore, this effect cannot account for the evolution of the skyrmion velocity and SkHA observed experimentally (Fig. 2). Furthermore, mechanisms involving a sizeable FL-SOT have been put forward to explain the drive dependence of the SkHA of slightly deformed skyrmions [16] or breathing skyrmions [45]. However, our micromagnetic simulations including both SOTs with realistic relative amplitudes (up to $C_{\text{FL}} = C_{\text{DL}}$) show no significant effect of the FL-SOT (see Sec. 2.2 within the Supplemental Material [27]). Finally, note that the Oersted field may also impact the measured SkHA, as

it generates a force on the skyrmion perpendicular to the current direction. For skyrmions with a core magnetized along $+\hat{\mathbf{z}}$, which corresponds to the condition of most of our experiments, this force is opposite to the gyrotropic force [12]. Thus, besides being of negligible amplitude, it may only reduce the measured SkHA and therefore cannot explain the pronounced drive dependence observed experimentally [Fig. 2(e)].

Another explanation to account for our experimental results is the presence of pinning sites in the material [22,23,35,36]. To include such an effect, we introduce disorder, modeled by a distribution of grains with different anisotropies [46,47]. The average grain size is 30 nm, a value in line with previous estimations in similar systems [23,24,26], and the anisotropy is varied randomly between $(1 \pm 0.05) K_u$. This approach has been shown to provide good qualitative agreement with experimental observations of the skyrmion statics under an applied field [22–26]. Figure 3(d) displays the motion of a skyrmion for a given disorder configuration and for $J = 6.7 \times 10^{11} \, \text{A m}^{-2}$. It reveals that the skyrmion experiences an additional dynamical deformation due to the local variation of anisotropy that creates minima for the DW energy. This makes it difficult to draw a distinction between the two contributions, namely that of the DL-SOT and that of the disorder. The skyrmion at rest is also distorted, since it relaxes on an inhomogeneous energy landscape, explaining the (static) deformation of some skyrmions in Fig. 1 [24–26]. Figures 3(e) and 3(f) display the skyrmion trajectories recorded for different grain distributions and for $J = 2.9 \times 10^{11} \, \text{A m}^{-2}$ and $J = 6.7 \times 10^{11} \, \text{A m}^{-2}$, respectively. The blue dotted lines represent the trajectories in the absence of disorder, which deviate slightly from linearity due to the skyrmion deformation. The first plot reveals a stochastic dynamics, with a large dispersion in the direction of motion. In some cases, the skyrmions are stopped on a strong pinning site, preventing further motion. For larger current densities, the number of such events decreases and the trajectory approaches that of the ideal case. This is emphasized in Fig. 4(a), which shows the skyrmion velocity as a function of the current density in the ideal case (blue dots) and the disordered case (black stars).

The disorder introduces different regimes in the skyrmion dynamics: at low driving current, the average velocity, calculated from the total displacement after a computation time of 8 ns, is close to zero. This pinned regime is highlighted by the shaded areas in Fig. 4. At higher current density, the force due to the current becomes large compared to the pinning force and the velocity increases and finally reaches the disorder-free velocity, defining the flow regime. This behavior is analogous to that of current-driven DWs [33] and highlights the fact that care should be taken when interpreting the regime of the skyrmion dynamics. In the pinned regime, a reduction in

the average SkHA is observed. Upon increasing the driving force, the SkHA increases monotonically and converges to the disorder-free SkHA in the flow regime. These results can be understood as follows: the pinning can be viewed as a force acting opposite to the ideal skyrmion motion direction [48], thus lowering its velocity. The gyrotropic response to this force will make the skyrmion deviate from its initial trajectory in a direction transverse to this pinning force, according to the second term of Eq. (1). This effect, referred to as extrinsic SkHE [22], prevails at low current density and becomes negligible as the force due to the current becomes sufficiently large as compared to the pinning force.

These results are in excellent agreement with our observations and strongly suggest that the observed drive dependence of the skyrmion velocity and that of the SkHA is largely due to pinning. Note that only the nonshaded areas in Fig. 4 are to be compared with the experimental results in Fig. 2. Although the critical current densities and skyrmion velocities for which the depinning and flow regimes are reached depend on the choice of disorder parameters [22,23,49], this approach constitutes a good qualitative description of the pinning effect on the current-driven skyrmion dynamics. Qualitatively, the micromagnetic simulations reveal that the disorder-free velocity and SkHA constitute upper bounds for the velocity and SkHA in disordered systems. This supports the aforementioned assumption of a lower damping in our film, which would increase the disorder-free velocity and the SkHA (Fig. 2, red dashed lines), leading to an excellent agreement with the simulations. Therefore, it confirms that the observed skyrmion dynamics are in a depinning regime and this suggests that the flow regime is reached for the largest current densities.

III. CONCLUSIONS

We have studied the current-driven dynamics of small magnetic skyrmions in an ultrathin Pt/Co/MgO film at room temperature. We observe that isolated magnetic skyrmions exhibit fast motion ($100 \ \mathrm{m \, s^{-1}}$) and a drive-dependent SkHE. Supported by a detailed characterization of the film properties and the SOTs governing the skyrmion dynamics, we show that these observations can be well accounted for by Thiele's model at high current density, which is particularly relevant in an ultrathin film hosting skyrmions with a well defined chirality. Micromagnetic simulations including the measured DL-SOT and FL-SOT as well as material inhomogeneities reproduce the different regimes of the drive-dependent skyrmion velocity and SkHA. This, in turn, allows us to rule out the impact of the FL-SOT on the skyrmion dynamics and to identify pinning as the dominant effect responsible for the drive dependence of the SkHE. Our results shed light on the current-driven skyrmion dynamics in ultrathin films, which paves the way

for future experimental investigations for the purpose of developing low-power skyrmion-based applications.

[1] A. Fert, V. Cros, and J. Sampaio, Skyrmions on the track, Nat. Nanotech. **8,** 152 (2013).

[2] X. Zhang, M. Ezawa, and Y. Zhou, Magnetic skyrmion logic gates: Conversion, duplication and merging of skyrmions, Sci. Rep. **5,** 9400 (2015).

[3] A. Bogdanov and A. Hubert, The stability of vortex-like structures in uniaxial ferromagnets, J. Magn. Magn. Mater. **195,** 182 (1999).

[4] J. Sampaio, V. Cros, S. Rohart, A. Thiaville, and A. Fert, Nucleation, stability and current-induced motion of isolated magnetic skyrmions in nanostructures, Nat. Nanotech. **8,** 839 (2013).

[5] W. Jiang, P. Upadhyaya, W. Zhang, G. Yu, M. B. Jungfleisch, F. Y. Fradin, J. E. Pearson, Y. Tserkovnyak, K. L. Wang, O. Heinonen, S. G. E. te Velthuis, and A. Hoffmann, Blowing magnetic skyrmion bubbles, Science **349,** 283 (2015).

[6] C. Moreau-Luchaire, C. Moutafis, N. Reyren, J. Sampaio, C. A. F. Vaz, N. V. Horne, K. Bouzehouane, K. Garcia, C. Deranlot, P. Warnicke, P. Wohlhüter, J.-M. George, M. Weigand, J. Raabe, V. Cros, and A. Fert, Additive interfacial chiral interaction in multilayers for stabilization of small individual skyrmions at room temperature, Nat. Nanotech. **11,** 444 (2016).

[7] O. Boulle *et al.*, Room-temperature chiral magnetic skyrmions in ultrathin magnetic nanostructures, Nat. Nanotech. **11,** 449 (2016).

[8] S. Woo, K. Litzius, B. Krüger, M.-Y. Im, L. Caretta, K. Richter, M. Mann, A. Krone, R. M. Reeve, M. Weigand, P. Agrawal, I. Lemesh, M.-A. Mawass, P. Fischer, M. Kläui, and G. S. D. Beach, Observation of room-temperature magnetic skyrmions and their current-driven dynamics in ultrathin metallic ferromagnets, Nat. Mater. **15,** 501 (2016).

[9] G. Yu, P. Upadhyaya, X. Li, W. Li, S. K. Kim, Y. Fan, K. L. Wong, Y. Tserkovnyak, P. K. Amiri, and K. L. Wang, Room-temperature creation and spin-orbit torque manipulation of skyrmions in thin films with engineered asymmetry, Nano Lett. **16,** 1981 (2016).

[10] A. Soumyanarayanan, M. Raju, A. L. G. Oyarce, A. K. C. Tan, M.-Y. Im, A. P. Petrović, P. Ho, K. H. Khoo, M. Tran, C. K. Gan, F. Ernult, and C. Panagopoulos, Tunable room-temperature magnetic skyrmions in Ir/Fe/Co/Pt multilayers, Nat. Mater. **16,** 898 (2017).

[11] S. Woo, K. M. Song, H.-S. Han, M.-S. Jung, M.-Y. Im, K.-S. Lee, K. S. Song, P. Fischer, J.-I. Hong, J. W. Choi, B.-C. Min, H. C. Koo, and J. Chang, Spin-orbit torque-driven skyrmion dynamics revealed by time-resolved x-ray microscopy, Nat. Commun. **8,** 15573 (2017).

[12] A. Hrabec, J. Sampaio, M. Belmeguenai, I. Gross, R. Weil, S. M. Chérif, A. Stashkevich, V. Jacques, A. Thiaville, and S. Rohart, Current-induced skyrmion generation and dynamics in symmetric bilayers, Nat. Commun. **8,** 15765 (2017).

[13] L. Caretta, M. Mann, F. Büttner, K. Ueda, B. Pfau, C. M. Günther, P. Hessing, A. Churikova, C. Klose, M. Schneider, D. Engel, C. Marcus, D. Bono, K. Bagschik, S. Eisebitt, and G. S. D. Beach, Fast current-driven domain walls and small skyrmions in a compensated ferrimagnet, Nat. Nanotech. **13,** 1154 (2018).

[14] S. Woo, K. M. Song, X. Zhang, Y. Zhou, M. Ezawa, X. Liu, S. Finizio, J. Raabe, N. J. Lee, S.-I. Kim, S.-Y. Park, Y. Kim, J.-Y. Kim, D. Lee, O. Lee, J. W. Choi, B.-C. Min, H. C. Koo, and J. Chang, Current-driven dynamics and inhibition of the skyrmion Hall effect of ferrimagnetic skyrmions in GdFeCo films, Nat. Commun. **9,** 959 (2018).

[15] W. Jiang, X. Zhang, G. Yu, W. Zhang, X. Wang, M. Benjamin Jungfleisch, J. E. Pearson, X. Cheng, O. Heinonen, K. L. Wang, Y. Zhou, A. Hoffmann, and S. G. E. te Velthuis, Direct observation of the skyrmion Hall effect, Nat. Phys. **13,** 162 (2017).

[16] K. Litzius, I. Lemesh, B. Krüger, P. Bassirian, L. Caretta, K. Richter, F. Büttner, K. Sato, O. A. Tretiakov, J. Förster, R. M. Reeve, M. Weigand, I. Bykova, H. Stoll, G. Schütz, G. S. D. Beach, and M. Kläui, Skyrmion Hall effect revealed by direct time-resolved x-ray microscopy, Nat. Phys. **13,** 170 (2017).

[17] W. Legrand, J.-Y. Chauleau, D. Maccariello, N. Reyren, S. Collin, K. Bouzehouane, N. Jaouen, V. Cros, and A. Fert, Hybrid chiral domain walls and skyrmions in magnetic multilayers, Sci. Adv. **4,** eaat0415 (2018).

[18] Y. Dovzhenko, F. Casola, S. Schlotter, T. X. Zhou, F. Büttner, R. L. Walsworth, G. S. D. Beach, and A. Yacoby, Magnetostatic twists in room-temperature skyrmions explored by nitrogen-vacancy center spin texture reconstruction, Nat. Commun. **9,** 2712 (2018).

[19] W. Li *et al.*, Anatomy of skyrmionic textures in magnetic multilayers, Adv. Mater. **31,** 1807683 (2019).

[20] I. Lemesh and G. S. D. Beach, Twisted domain walls and skyrmions in perpendicularly magnetized multilayers, Phys. Rev. B **98,** 104402 (2018).

[21] W. Legrand, N. Ronceray, N. Reyren, D. Maccariello, V. Cros, and A. Fert, Modeling the Shape of Axisymmetric Skyrmions in Magnetic Multilayers, Phys. Rev. Appl. **10,** 064042 (2018).

[22] J.-V. Kim and M.-W. Yoo, Current-driven skyrmion dynamics in disordered films, Appl. Phys. Lett. **110,** 132404 (2017).

[23] W. Legrand, D. Maccariello, N. Reyren, K. Garcia, C. Moutafis, C. Moreau-Luchaire, S. Collin, K. Bouzehouane, V. Cros, and A. Fert, Room-temperature current-induced generation and motion of sub-100 nm skyrmions, Nano Lett. **17,** 2703 (2017).

[24] K. Zeissler, M. Mruczkiewicz, S. Finizio, J. Raabe, P. M. Shepley, A. V. Sadovnikov, S. A. Nikitov, K. Fallon, S. McFadzean, S. McVitie, T. A. Moore, G. Burnell, and C. H. Marrows, Pinning and hysteresis in the field dependent diameter evolution of skyrmions in Pt/Co/Ir superlattice stacks, Sci. Rep. **7,** 15125 (2017).

[25] R. Juge, S.-G. Je, D. de Souza Chaves, S. Pizzini, L. D. Buda-Prejbeanu, L. Aballe, M. Foerster, A. Locatelli, T. O. Menteş, A. Sala, F. Maccherozzi, S. S. Dhesi, S. Auffret, E. Gautier, G. Gaudin, J. Vogel, and O. Boulle, Magnetic skyrmions in confined geometries: Effect of the magnetic field and the disorder, J. Magn. Magn. Mater. **455,** 3 (2018).

[26] I. Gross, W. Akhtar, A. Hrabec, J. Sampaio, L. J. Martínez, S. Chouaieb, B. J. Shields, P. Maletinsky, A. Thiaville, S. Rohart, and V. Jacques, Skyrmion morphology in ultrathin magnetic films, Phys. Rev. Mater. **2,** 024406 (2018).

[27] See the Supplemental Material at http://link.aps.org/supplemental/10.1103/PhysRevApplied.12.044007 for the sample characterization, the determination of the parameters listed in Table I, and micromagnetic simulations performed for different values of the FL-SOT in the absence of disorder.

[28] A. A. Thiele, Steady-State Motion of Magnetic Domains, Phys. Rev. Lett. **30,** 230 (1973).

[29] M.-H. Nguyen, D. C. Ralph, and R. A. Buhrman, Spin Torque Study of the Spin Hall Conductivity and Spin Diffusion Length in Platinum Thin Films with Varying Resistivity, Phys. Rev. Lett. **116,** 126601 (2016).

[30] A. A. Thiele, Applications of the gyrocoupling vector and dissipation dyadic in the dynamics of magnetic domains, J. Appl. Phys. **45,** 377 (1974).

[31] In a previous work, we observed, using XMCD-PEEM, that the skyrmion profile in Pt/Co/MgO is fitted well by a 360° Bloch-wall profile [7].

[32] R. Tomasello, E. Martinez, R. Zivieri, L. Torres, M. Carpentieri, and G. Finocchio, A strategy for the design of skyrmion racetrack memories, Sci. Rep. **4,** 6784 (2014).

[33] I. M. Miron, T. Moore, H. Szambolics, L. D. Buda-Prejbeanu, S. Auffret, B. Rodmacq, S. Pizzini, J. Vogel, M. Bonfim, A. Schuhl, and G. Gaudin, Fast current-induced domain-wall motion controlled by the Rashba effect, Nat. Mater. **10,** 419 (2011).

[34] C. Reichhardt, D. Ray, and C. J. O. Reichhardt, Quantized transport for a skyrmion moving on a two-dimensional periodic substrate, Phys. Rev. B **91,** 104426 (2015).

[35] C. Reichhardt, D. Ray, and C. J. O. Reichhardt, Collective Transport Properties of Driven Skyrmions with Random Disorder, Phys. Rev. Lett. **114,** 217202 (2015).

[36] C. Reichhardt and C. J. O. Reichhardt, Noise fluctuations and drive dependence of the skyrmion Hall effect in disordered systems, New J. Phys. **18,** 095005 (2016).

[37] P. J. Metaxas, J. P. Jamet, A. Mougin, M. Cormier, J. Ferré, V. Baltz, B. Rodmacq, B. Dieny, and R. L. Stamps, Creep and Flow Regimes of Magnetic Domain-Wall Motion in

Ultrathin Pt/Co/Pt Films with Perpendicular Anisotropy, Phys. Rev. Lett. **99,** 217208 (2007).

[38] T. H. Pham, J. Vogel, J. Sampaio, M. Vaňatka, J.-C. Rojas-Sánchez, M. Bonfim, D. S. Chaves, F. Choueikani, P. Ohresser, E. Otero, A. Thiaville, and S. Pizzini, Very large domain wall velocities in Pt/Co/GdOx and Pt/Co/Gd trilayers with Dzyaloshinskii-Moriya interaction, EPL **113,** 67001 (2016).

[39] H. Min, R. D. McMichael, M. J. Donahue, J. Miltat, and M. D. Stiles, Effects of Disorder and Internal Dynamics on Vortex Wall Propagation, Phys. Rev. Lett. **104,** 217201 (2010).

[40] J.-M. L. Beaujour, J. H. Lee, A. D. Kent, K. Krycka, and C.-C. Kao, Magnetization damping in ultrathin polycrystalline Co films: Evidence for nonlocal effects, Phys. Rev. B **74,** 214405 (2006).

[41] K.-W. Kim, J.-H. Moon, K.-J. Lee, and H.-W. Lee, Prediction of Giant Spin Motive Force due to Rashba Spin-Orbit Coupling, Phys. Rev. Lett. **108,** 217202 (2012).

[42] J.-V. Kim, Role of nonlinear anisotropic damping in the magnetization dynamics of topological solitons, Phys. Rev. B **92,** 014418 (2015).

[43] A. V. Khvalkovskiy, V. Cros, D. Apalkov, V. Nikitin, M. Krounbi, K. A. Zvezdin, A. Anane, J. Grollier, and A. Fert, Matching domain-wall configuration and spin-orbit torques for efficient domain-wall motion, Phys. Rev. B **87,** 020402 (2013).

[44] L. D. Buda, I. L. Prejbeanu, U. Ebels, and K. Ounadjela, Micromagnetic simulations of magnetisation in circular cobalt dots, Comput. Mater. Sci. **24,** 181 (2002).

[45] R. Tomasello, A. Giordano, S. Chiappini, R. Zivieri, G. Siracusano, V. Puliafito, I. Medlej, A. La Corte, B. Azzerboni, M. Carpentieri, Z. Zeng, and G. Finocchio, Micromagnetic understanding of the skyrmion Hall angle current dependence in perpendicularly magnetized ferromagnets, Phys. Rev. B **98,** 224418 (2018).

[46] M. Voto, L. Lopez-Diaz, and L. Torres, Effects of grain size and disorder on domain wall propagation in CoFeB thin films, J. Phys. D: Appl. Phys. **49,** 185001 (2016).

[47] F. Garcia-Sanchez, J. Sampaio, N. Reyren, V. Cros, and J.-V. Kim, A skyrmion-based spin-torque nano-oscillator, New J. Phys. **18,** 075011 (2016).

[48] J. Iwasaki, M. Mochizuki, and N. Nagaosa, Universal current-velocity relation of skyrmion motion in chiral magnets, Nat. Commun. **4,** 1463 (2013).

[49] A. Salimath, A. Abbout, A. Brataas, and A. Manchon, Current-driven skyrmion depinning in magnetic granular films, Phys. Rev. B **99,** 104416 (2019).

[50] L. Aballe, M. Foerster, E. Pellegrin, J. Nicolas, and S. Ferrer, The ALBA spectroscopic LEEM-PEEM experimental station: Layout and performance, J Synchrotron Rad. **22,** 745 (2015).

[51] M. Foerster, J. Prat, V. Massana, N. Gonzalez, A. Fontsere, B. Molas, O. Matila, E. Pellegrin, and L. Aballe, Custom sample environments at the ALBA XPEEM, Ultramicroscopy **171,** 63 (2016).

[52] T. O. Menteş, G. Zamborlini, A. Sala, and A. Locatelli, Cathode lens spectromicroscopy: Methodology and applications, Beilstein J. Nanotechnol. **5,** 1873 (2014).

Correction: The units for the last two columns in Table 1 were incomplete and have been fixed.